International Journal of Medical, Medicine and Health Sciences
ISSN: 2517-9969
Vol:1, No:3, 2007

Left Ventricular Model to Study the Combined Viscoelastic, Heart Rate, and Size Effects

Elie H. Karam[(1)], and Antoine B. Abche[(2)]

Abstract**—**It is known that the heart interacts with and adapts to its venous and arterial loading conditions. Various experimental studies and modeling approaches have been developed to investigate the underlying mechanisms. This paper presents a model of the left ventricle derived based on nonlinear stress-length myocardial characteristics integrated over truncated ellipsoidal geometry, and second-order dynamic mechanism for the excitation-contraction coupling system. The results of the model presented here describe the effects of the viscoelastic damping element of the electromechanical coupling system on the hemodynamic response. Different heart rates are considered to study the pacing effects on the performance of the left-ventricle against constant preload and afterload conditions under various damping conditions. The results indicate that the pacing process of the left ventricle has to take into account, among other things, the viscoelastic damping conditions of the myofilament excitation-contraction process. The effects of left ventricular dimensions on the hemdynamic response have been examined. These effects are found to be different at different viscoelastic and pacing conditions.

Keywords**—**Myocardial sarcomere, cardiac pump, excitation-contraction coupling, viscoelasicity

I. INTRODUCTION

DIFFERENT approaches have been followed in the modeling of the left-ventricular pump. Some of these approaches are: lumped time-varying elastance [1], finite element [2], and geometric integration of muscle characteristics [3], [4], [5]. The original model of our work [3], [4] has been built from serial and parallel arrangement of sarcomere units. Each sarcomere unit consists of parallel active and passive elements that were described by nonlinear stress-length functions. The myocardial functions were integrated over a cylindrical geometry of the structure to obtain the global left ventricular function. Time-variation was introduced via a lumped periodic excitation-contraction coupling mechanism of the myocardial fibers. The cardiovascular lumped system consisting of the left ventricular model with its venous preload and arterial load was used to study left ventricular hemodynamics, energetics, and physiological hypertrophy for varying chronic load conditions.

II. DERIVATION OF THE MODIFIED MODEL

Manuscript received June 5, 2006.
(1) E. H. Karam is with the University of Balamand. P.O.Box 100, Tripoli, LEBANON (phone: 961-6930250; fax: 961-6930238; email: elie.karam@balamand.edu.lb)
(2) A. B. Abche is with the University of Balamand. P.O.Box 100, Tripoli, LEBANON (email: antoine.abche@balamand.edu.lb)

In this work, a new relationship between ventricular pressure and volume is derived from myocardial properties integrated over a truncated ellipsoidal geometry.

The Myocardial Unit

The myocardial sarcomere is the essential force producing element in the heart. It consists of a parallel arrangement of actin and myosin fibrils (Fig.1). The Ca^{++} concentration ($[Ca^{++}]$) controls the longitudinal force produced by these fibers in the process known as the excitation-contraction coupling mechanism [6].

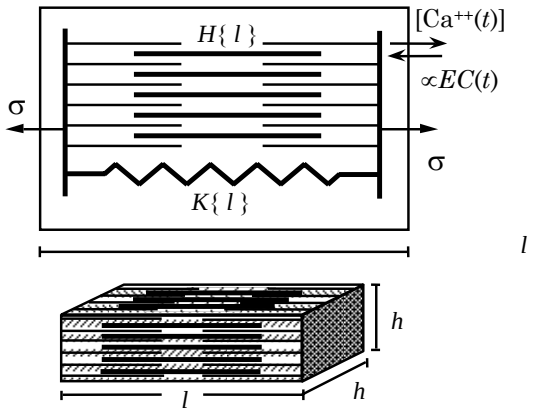

Fig. 1 Model of the cardiac sarcomere unit. Upper drawing: functional structure consisting of the actin-myosin sliding filaments and an elastic element due to elastin and collagen connective mesh. Lower drawing represents a rectangular volume unit which embodies the sarcomere structure and prescribes the dimensions of the element.

Experiments have been performed to obtain the function of the sarcomere. For example, the time development of muscle force (Fig.2a) originates from the periodic increase (release) and decrease (uptake) in $[Ca^{++}]$. The peak muscle force is found to increase with increasing muscle length (Fig.2b) i.e., the Starling law for muscle [7]. A maximum force occurs at an optimal length, thought to be the position of optimal fiber overlap.

The model of the sarcomere unit consists of two basic elements: active contractile and passive elastic elements, arranged in parallel (Fig.1). The active element provides the force-generating mechanism, while the passive component imparts the stiffness to the sarcomere. The level of force

produced by the contractile unit model is determined by the excitation-contraction coupling mechanism, which is a function of the time-varying [Ca^{++}] and muscle contractility. This function is responsible for the shape of the isometric muscle force curve (Fig.2a). This is indicated in Figure 1 by a time-varying level of [Ca^{++}] in a volume surrounding the sarcomere unit. The level of the force produced is modulated by the length of the contractile unit at any given time, according to the Starling law (Fig.2b).

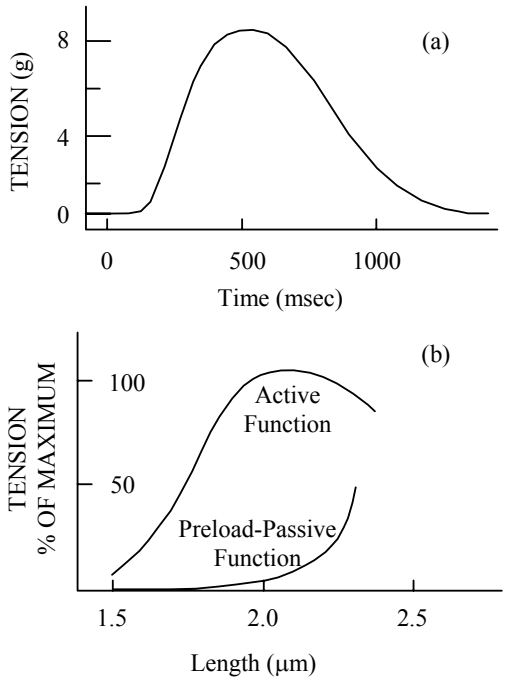

Fig. 2 (a) The time dependent isometric development of myocardial force [Modified from Parmley *et al*., 1969]. (b) Active and passive cardiac muscle force-length curves [Modified from Ross *et al*., 1967].

The Excitation-Contraction Function

The sarcomere model can be transformed into its proper mathematical form. Normalization of the measured tension by the peak isometric tension yields the time-dependent normal muscle stress, *EC*(*t*), known as the excitation-contraction function. The time-varying shape of the EC(t) function is assumed to be independent of length.

For isovolumic beats, it has been found that the time-dependence of ventricular pressure can be represented by a sinusoid [8]. However, this function was not apparently sufficient, and an exponential decay function, for example, has been added to the sinusoidal function [13].

In the current work, the excitation-contraction function is derived using a second order dynamic system approach (fig. 3a). The system consists of [Ca^{++}] activation-deactivation periodic function, $E_{in}(t)$, that serves as an input (stimulus) to a second order electromechanical system. The stimulus is represented by different constant activation and deactivation rates. The response of the system is a normalized excitation-contraction function, *EC*(*t*). The second order system is conceived from the process of filament mass acceleration in the viscoelastic medium of the contractile element (Fig. 3b).

Length Modulation

The Starling stress-length relationship of a muscle unit (Fig. 2b) is defined as the general function $H\{l, l_a\}$, where l is the actual muscle length and l_a is the minimal muscle length at which the active stress drops to zero. The active stress, $\sigma_a\{t, l\}$, developed by a given myofibril can be written as a product of the excitation-contraction function and the modulating Hill relation,

$$\sigma_a\{t, l\} = EC(t)\cdot H\{l, l_a\} \quad (1)$$

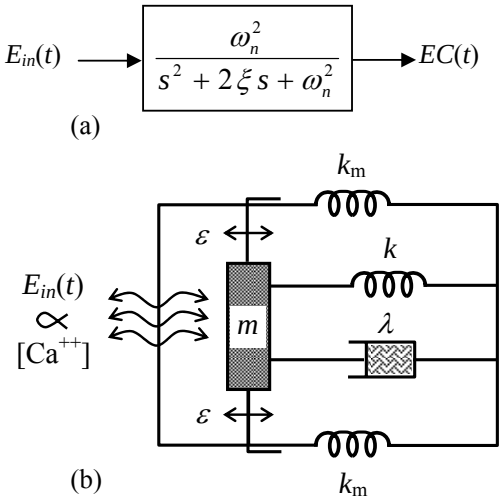

Fig. 3 (a) Second-order dynamic system used as a model of the excitation-contraction process. (b) Electrochemical-mechanical structure used to derive model dynamic function for the excitation-contraction process. The parameters used have the following representation: $\varepsilon \equiv$ relative change in sarcomere length; k, $\lambda \equiv$ viscoelastic coefficients of the sarcomere inner structure; $k_m \equiv$ elastic coefficient of the filament membrane; and finally, $E_{in}(t) \propto [Ca^{++}]$ represents the electrochemical stimulation-calcium flow process.

The functions in (Eq.1) have been measured for different animals and are available in the literature [9]. The most appropriate relationship for the active stress-length function of the muscle is not clear, since linearity has been mostly applied. However, muscle physiology dictates that nonlinear function must apply. For lack of the true stress-length function, a second-order polynomial was assumed for $H\{l, l_a\}$ to proceed with the analysis.

$$H\{l, l_a\} = a(l-l_a)^2 + b(l-l_a) \quad (2)$$

where a and b are constants that can be evaluated from muscle data.

The stress developed by the passive fibers of the sarcomere unit is, by definition, independent of time. This passive stress can be measured when the active elements are

not stimulated (Fig.2b) and has been found to be primarily a function of the muscle length. Thus, the passive sarcomere unit behaves as a spring with a nonlinear elastic response and is defined by a general function $K\{l, l_o\}$, where l_o is the resting length or zero-stress length. This function can be analytically represented or replaced with the proper muscle data obtained from the literature.

The passive stretch of muscle has been shown to follow an exponential stress-length relationship ([10]. In our work, a nonlinear muscle stress-length law was incorporated, where $K\{l–l_o\}$ has been represented by an exponential function in terms of the length l.

$$K\{l, l_o\} = \alpha\{\exp[\beta(l–l_o)] – 1\} \quad (3)$$

where, α and β are empirical constants determined from muscle data.

Finally, the total stress developed by the contractile unit model can be obtained as

$$\sigma\{t, l\} = EC(t)\cdot H\{l, l_a\} + K\{l, l_o\} \quad (4)$$

Left Ventricular Geometry

A 3-D array of myocardial units that has been previously arranged into a cylindrical geometry [3], [4] is now replaced by a truncated ellipsoidal geometry chosen to represent the structure of the ventricle (Fig.4) in the derivation of the new nonlinear pressure-volume function.

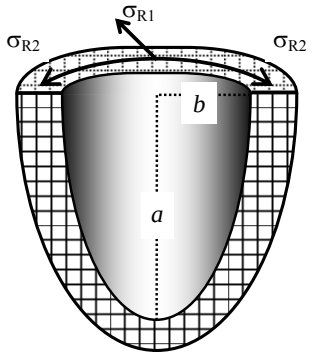

Fig. 4 A truncated ellipsoid, representing the shape of the left ventricle, where "*a*" is the major semi-axis, "*b*" is minor semi-axis, and "σ_{R1}" and "σ_{R2}" are the longitudinal and circumferential stresses, respectively.

By combining geometric functions with stress-length and stress-pressure relationships, the global left-ventricular pressure-volume is obtained, i.e.,

$$P(t) = P_g(t, V) + P_c(V) \quad (5)$$

In Equation (5), $P_g(t, V)$ and $P_c(V)$ represent the active and passive pressure-volume characteristics of the left ventricle, respectively. P_g and P_c have nonlinear expressions with respect to volume. P_g depends on time and volume, whereas P_c depends only on volume.

The actual physiological preload to the left ventricle has been lumped, since the interaction among its various compartments is not a subject of this work. This lumped preload system is represented in the physical prototype model (Fig.5) by a filling reservoir connected to the left ventricle via a resistive tube. The pressure of the fluid in the filling reservoir represents the mean filling pressure, P_p, of the left ventricle. The resistance of the filling tube, R_p, represents the lumped value of the flow resistance of the pulmonary venous return and inflow tract.

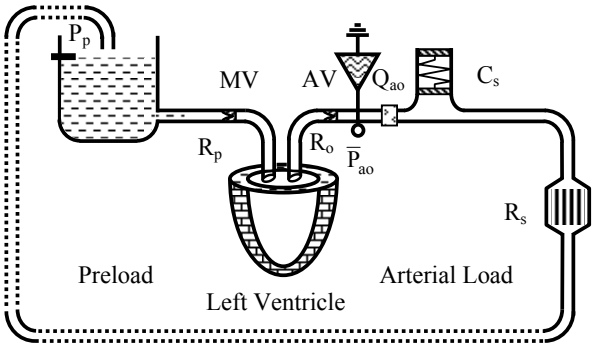

Fig. 5 Prototype model of the cardiovascular system. The left ventricle ellipsoid model is connected to the preload and the afterload models of the cardiovascular system. Here, $\bar{P}_{ao}$ is the value of the mean aortic pressure to which the left ventricle is adjusting.

The arterial load system represents the arterial system, from the root aorta up to systemic vasculature. In the prototype and analog equivalent circuit (Figs. 5 and 6), the arterial load is represented by the modified Windkessel model consisting of the impedance at the root aorta, Z_O, the total systemic compliance, C_S, and the total peripheral resistance, R_S. The system equations obtained from the analog model (Fig. 6) are:

$$\frac{dP_c}{dt} = \frac{1}{C_v}\left(\frac{P_P - P_v}{R_P + R_{mv}} - \frac{P_v - P_s}{R_o + R_{av}}\right) \quad (6)$$

$$\frac{dP_s}{dt} = \frac{1}{C_s}\left(\frac{P_v - P_s}{R_o + R_{av}} - \frac{P_s}{R_s}\right) \quad (7)$$

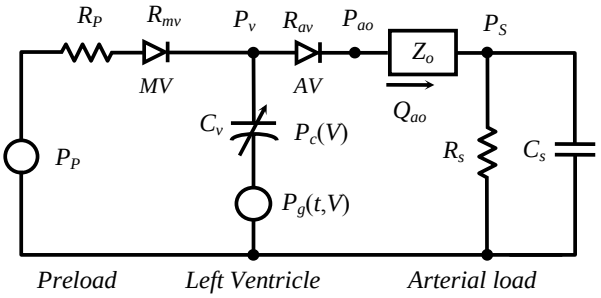

Fig. 6 Analog circuit representing the proposed model of the left ventricle connected to the preload and afterload counterparts of the cardiovascular system (eee text for details).

In equations (6 and 7) R_{mv} and R_{av} represent valve resistances, which are functions of the pressure gradient across them. The system response is obtained numerically, using Newton-Raphson root-solving and fourth-order Runge-Kutta integration algorithms. Thus, the instantaneous values of the ventricular and systemic pressures can be determined. Then, the corresponding mitral flow (Q_m), aortic flow (Q_{ao}), aortic pressure (P_{ao}), stroke volume (SV), end-diastolic volume (EDV), end-systolic volume (SV), cardiac output (CO), and ejection fraction are solved for.

III. RESULTS

The effects of the electromechanical damping conditions on the hemodynamic response of paced left ventricle are examined with this model.

Basic Hemodynamic Response

The effects of the viscoelastic damping conditions on the hemodynamic response of paced left ventricle are examined with this model. The hemodynamic response of the modified excitation-contraction system is shown below for a range of damping ratio, ζ (zeta) values and fixed heart rate.The pressure and volume waveforms obtained from the model are shown in Figure 7, with the left-ventricular P-V loops. The results indicate that the damping element of the electromechanical excitation-contraction process has significant effects on the pressure and volume waveforms. Low values of the damping ratio, ζ, lead to very fast blood ejection and oscillation in the LV systolic pressure. The diastolic phase is also affected by low values of ζ, where pressure oscillations and phase filling of different rates are observed. As the damping ratio increases, the oscillations in systolic pressure disappear, while the ejection rate becomes slower, extending a little longer in time, with slow ejection rate occurring toward the end of the ejection interval. As the damping ratio is further increased, the isovolumic contraction interval increases, leading to a decrease of the end-diastolic volume under constant rate of pacing conditions.

The effects on the pressure and volume waveforms are reflected onto the pressure-volume loop. As the viscoelastic damping ratio is increased, the P-V loop is reduced with lower end-diastolic volume and lower pressure during ejection. However, it can be observed that the end-diastolic volume did not change significantly for ζ between 0.3 and 1.1. Also, the ejection at lower values of ζ occurs at a faster rate compared to that at higher values of ζ. A reduced P-V loop area suggests lower work performed by the left ventricle. It is important to indicate here that this change in the value of ζ is applied at a constant heart rate (HR) value of 75 beats/min and without any compensation mechanism. In the actual cardiovascular system, the effect of the viscoelastic damping element would interact with short-term and long-term regulation and compensation mechanisms.In Figure 8, the effects of ζ are examined for different values of HR. In general, the effects of increased value of ζ appear to be more intensified at higher HR levels. The hemodynamic response variables shown are end-diastolic volume (EDV), ejection fraction (EF), cardiac output (CO), and mean systemic pressure (MAP).

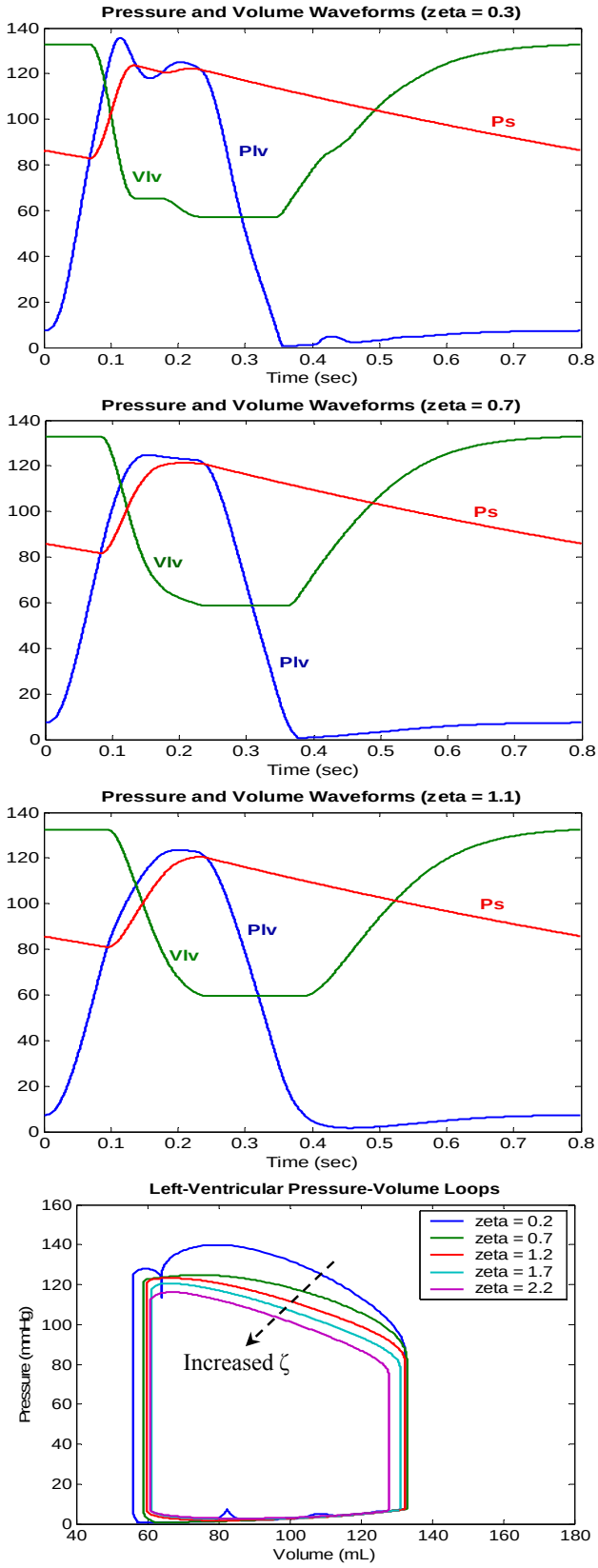

Fig. 7 LV pressure (Plv), systemic pressure (Psys), LV volume (Vlv), and pressure-volume loops for damping ratio 0.3, 0.7, and 1.1.

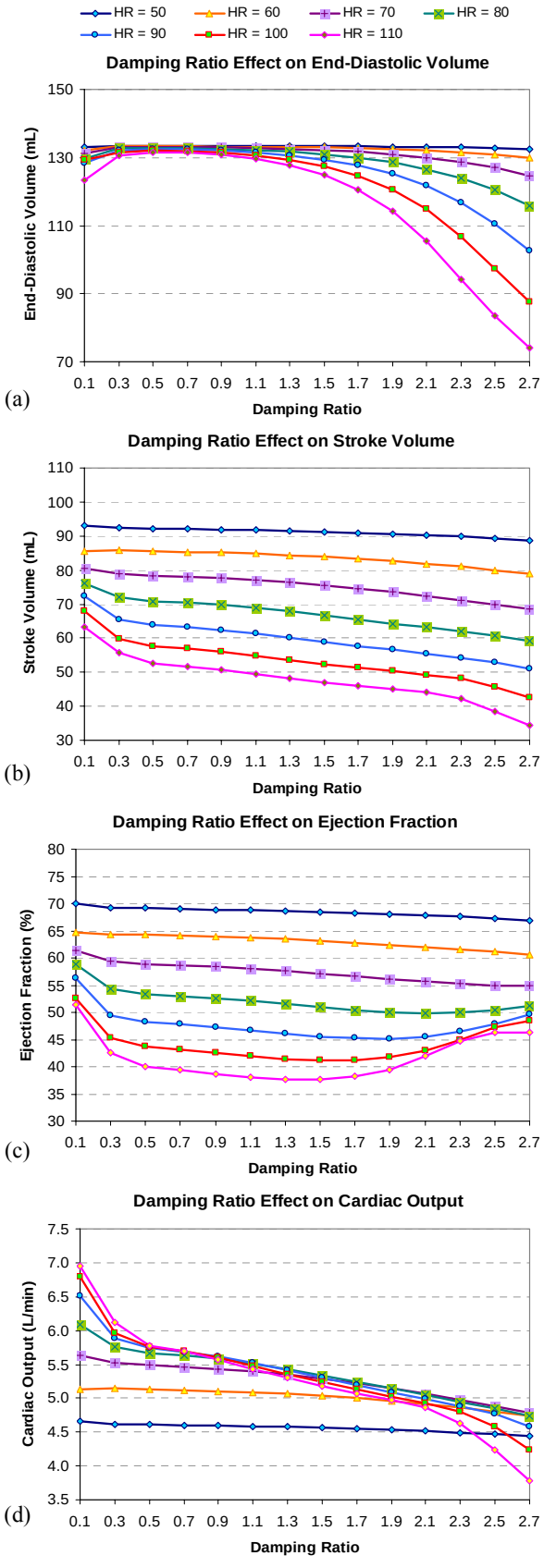

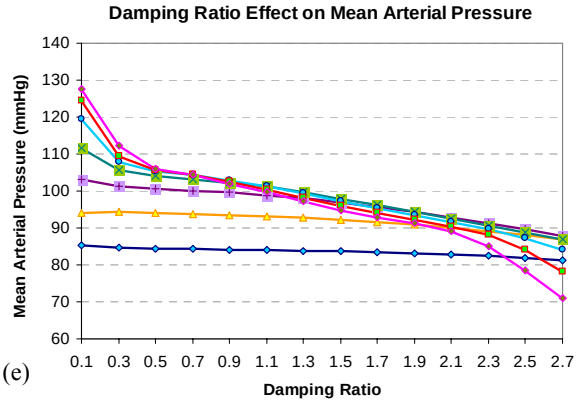

Fig. 8 Hemodynamic response variable variations with variation of damping ratio in the range 0.1 to 2.3

The EDV curves (Fig.8a) indicate that at high HR and high values of ζ, the EDV is significantly reduced. This reduction cannot be attributed to HR alone or ζ alone. In fact, at low HR values (between 50 and 60 beats/min), EDV is relatively independent of ζ. And over some range of ζ (0.4 to 0.8 for the case here), different HR values result in very small changes in EDV. High values of HR imply less time for filling, yet this phenomenon is intensified at high viscoelastic damping ratio conditions.

While a ζ range exists over which HR-induced variations in EDV are not significant, this is not the case for SV (Fig.8b) which seems to be highly affected by the variations of ζ and HR. At low HR values the SV undergoes a small decrease with ζ. The results show that the slope of decrease in SV with ζ gets larger at higher HR values. It can be observed also that at high HR and large damping, the decrease in SV starts to take a sharper drop.

The combined effects of HR and ζ on the EDV and SV extend onto the EF or the ratio of SV over EDV. In general, EF decreases with ζ. The decrease is small at low HR levels, and it becomes more significant at higher levels of HR. The small increase in EDV at low range of ζ combined with the decrease in SV results in decrease of EF (Fig.8c). On the other hand, the EDV drops significantly in the upper range of ζ at high HR values, whereas the SV drop over this range is rather linear. This is reflected in the observed increase in EF at the upper range of ζ for the high HR values.

Now, while the SV is generally lower at high HR, the reduction in SV is compensated for by the HR when it comes to the estimation of CO (Fig.8d). Thus the CO levels are generally higher at high HR values. In general, the CO decrease over the range of ζ becomes more significant as HR level is increased. It can be observed that as the viscous damping gets larger, the HR compensation becomes less effective in indication of the higher energy losses and lower output, therefore lower efficiency.

The variations in CO over the range of ζ and at different HR levels have high degree of correlation with those in the MAP (Fig.8e). This shows that, while the model is highly nonlinear and pulsatile, the well known relationship among

MAP, CO, and total peripheral resistance (TPR), kept fixed in this case, is still holding here, i.e.,

MAP (mmHg) = CO (mL/sec) × TPR (mmHg·sec/mL).

In fact, the TPR is calculated for each value of zeta at different HR conditions. The results are shown in Fig.9. The actual value of systemic resistance used in the model simulation is 1.10 mmHg·sec/mL. A small deviation (about 2%) in the calculated value of TPR relative to the actual value is observed at high HR and large damping.

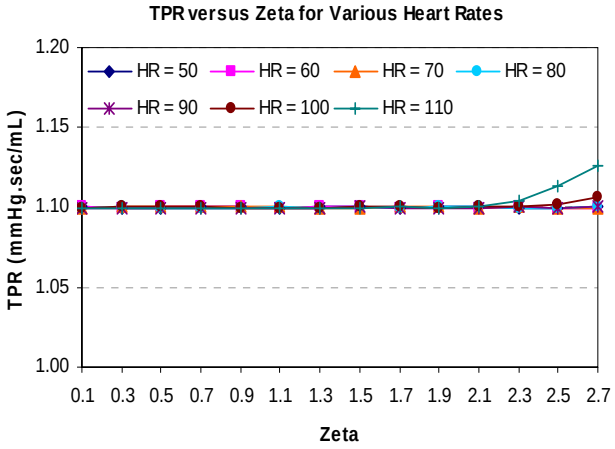

Fig. 9 TPR values calculated from MAP and CO results for each value of zeta at different HR conditions; the actual value of systemic resistance used in the model simulation is 1.10 mmHg·sec/mL

Size Effects

For an adult, whose body growth has stabilized, the hemodynamic loading conditions would be expected to be invariant. Over a long time period the heart can then adapt by altering its dimensions. Hence, the effect of altered cardiac size on cardiac function with fixed filling and arterial systems was examined. While in actual physiological cases, heart rate variation might take place within the short-term regulation condition, constant heart rate is used in this protocol, in order to examine the effect of cardiac pacing.

Cardiac adaptation is modelled by changing the wall-thickness and circumference of the left-ventricle. The length of the ventricle is assumed to be constant approximately for the range studied. In fact, the effect of the valve to apex length does not alter the qualitative aspects of the results. Filling and arterial load elements are fixed at control levels. End-diastolic volume, systolic, diastolic and mean arterial diastolic pressures, stroke volume, ejection fraction, and cardiac output were evaluated from the model as a function of wall-thickness. A family of curves is obtained for different values of circumference (Figures 10, 11, and 12).

The effects of the left ventricular wall-thickness and mid-wall circumference have been examined for different heart rate conditions (50 to 110 BPM) and two values of damping conditions 0.4 and 2.0). The hemodynamic response obtained under these various conditions is illustrated in Figures 10, 11, and 12 in terms of end-diastolic volume, stroke-volume, and mean arterial pressure, respectively.

Figure 10a shows the variation of the end-diastolic volume (EDV) with wall-thickness (range from 0.4 to 2.7 cm) under various heart rate conditions (50 to 110 BPM) for three different values of mid-wall circumference (15.0, 18.0, and 21.0 cm) and damping ratio equal to 0.4. The results here indicate that the EDV is independent of HR over the examined range of wall-thickness, and the relatively low damping value of 0.4. However, it can be seen that the EDV decreases with increased levels of wall-thickness. The results also indicate that as the left-ventricle mid-wall circumference dilates from 15.0 to 18.0, the EDV increases by almost 50%; and as the left-ventricle mid-wall circumference dilates from 18.0 to 21.0, the EDV increases by about 38%.

Figure 10b shows for the same conditions mentioned above, the variation of the EDV with wall-thickness (range from 0.4 to 2.7 cm), except that the damping ratio is equal now to 2.0. The results are similar to those seen in Figure 10a, with one main difference. It can be observed that the decrease of EDV with wall-thickness becomes larger with relatively higher rate of pacing conditions, especially toward the upper range of wall-thickness. This relative decrease in EDV could be mainly due to the constant available filling energy attempting to fill a heavier left-ventricle under relatively higher levels of viscous energy losses.

Figure 11a shows the variation of the stroke-volume (SV) with wall-thickness (range from 0.4 to 2.7 cm) under same conditions of Figure 10a. The results here indicate that the SV exhibits certain maximization with respect wall-thickness. The maximum SV value is higher at lower heart rate levels; however, the wall-thickness value at the maximum SV occurs is lower at lower HR values. The same pattern repeats as the mid-wall circumference is increased. However, the pattern is shifted to higher wall-thickness values at higher mid-wall circumferences.

The ratio of wall-thickness over mid-wall circumference at which the SV maxima occur is not constant. For HR = 50 BPM, for example, the ratio changes from 0.067 to 0.089 to 0.10 corresponding respectively to the mid-wall circumference values 15.0, 18.0, and 21.0 cm.

Figure 11b shows – for the same conditions mentioned above, the variation of the SV with wall-thickness, except that the damping ratio is equal now to 2.0. The results show similar patterns to those seen in Figure 11a, with two main differences. At low HR values, the SV has approximately the same maximum value. This maximum SV value is reduced at higher HR levels. On the other hand, the wall-thickness at which the maximum SV occurs is lower at higher damping ratio. Again, this reduction could be due to the under relatively higher levels of viscous energy losses.

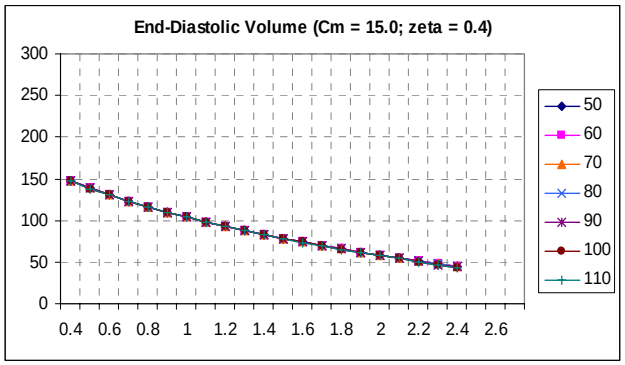

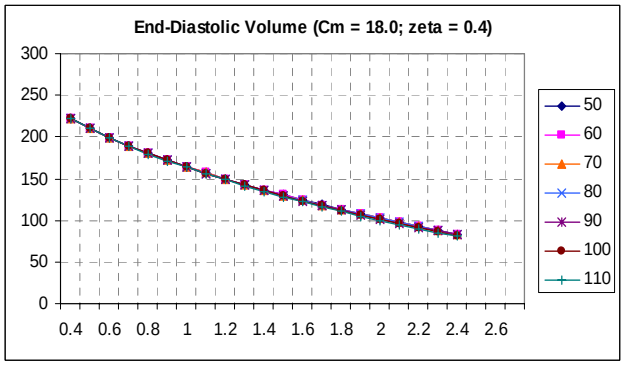

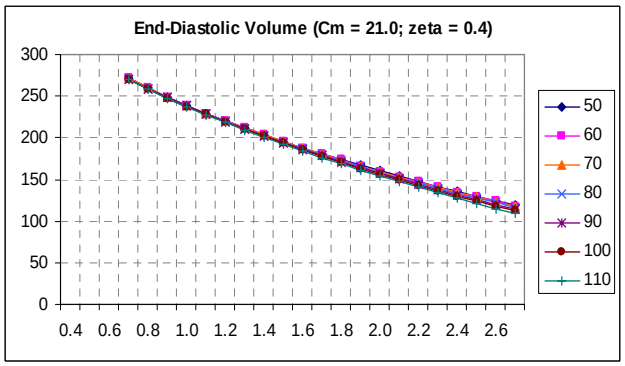

Fig. 10a Variation of the end-diastolic volume (EDV) with wall-thickness (range from 0.4 to 2.7 cm) under various heart rate conditions (50 to 110 BPM) for three different values of mid-wall circumference (15.0, 18.0, and 21.0 cm) and damping ratio equal to 0.4.

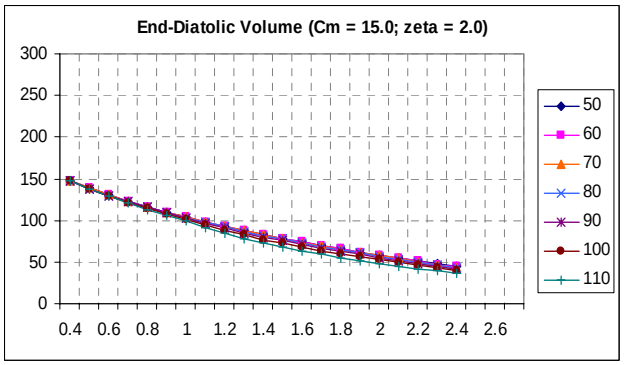

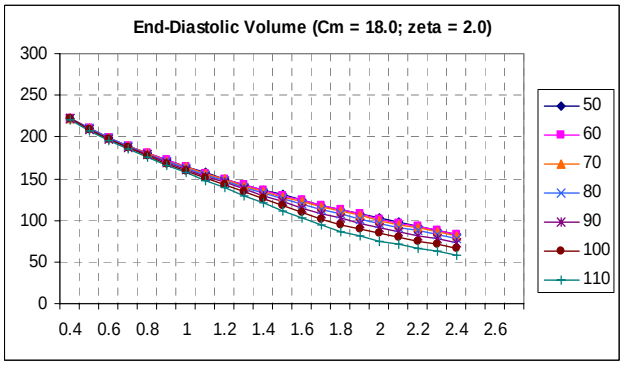

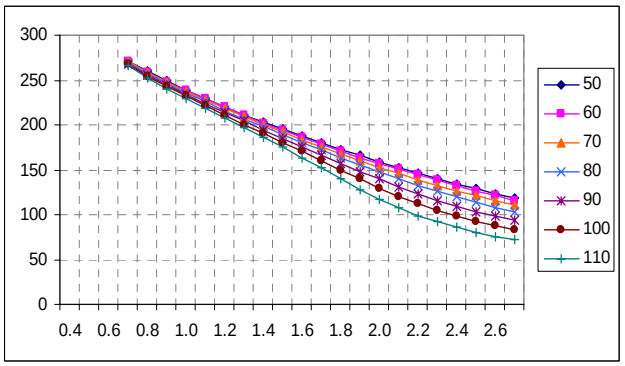

Fig. 10b Variation of the end-diastolic volume (EDV) with wall-thickness (range from 0.4 to 2.7 cm) under various heart rate conditions (50 to 110 BPM) for three different values of mid-wall circumference (15.0, 18.0, and 21.0 cm) and damping ratio equal to 2.0.

Figure 12a shows the variation of the mean-arterial pressure (MAP) with wall-thickness under same conditions of Figure 10a. Similar to the case of SV, the results here indicate that the MAP exhibits certain maximization with respect wall-thickness. However, the maximum MAP value is lower at lower heart rate levels. Yet, the wall-thickness value at the maximum SV occurs is lower at lower HR values. The same pattern repeats as the mid-wall circumference is increased. However, the pattern is shifted to higher wall-thickness values at higher mid-wall circumferences. Two features distinguish the MAP variations here compared to those of SV. The SV variations with HR are large at low wall-thickness and relatively small at high wall-thickness. The opposite variations are observed for the case of MAP.

The second distinctive feature in MAP compared to SV variations is the value at which the maxima occur. The results from this model indicate that the MAP maximum occurs at higher wall-thickness compared to that of SV.

Figure 12b shows – for the same conditions mentioned above, the variation of the MAP with wall-thickness, except that the damping ratio is equal now to 2.0. The results show similar patterns to those seen in Figure 12a, with two main differences. At low HR values, the MAP has approximately the same maximum value. This maximum MAP value is reduced at higher HR levels. On the other hand, the wall-thickness at which the maximum MAP occurs is lower at higher damping ratio. Again, this reduction could be due to the under relatively higher levels of viscous energy losses.

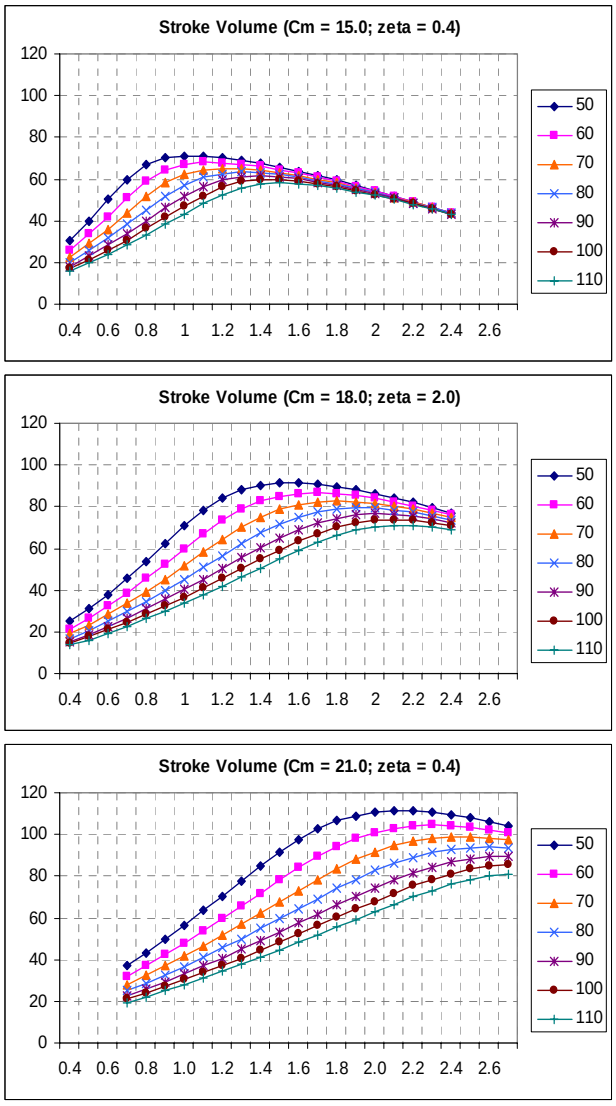

Fig. 11a Variation of the stroke-volume (SV) with wall-thickness (range from 0.4 to 2.7 cm) under various heart rate conditions (50 to 110 BPM) for three different values of mid-wall circumference (15.0, 18.0, and 21.0 cm) and damping ratio equal to 0.4

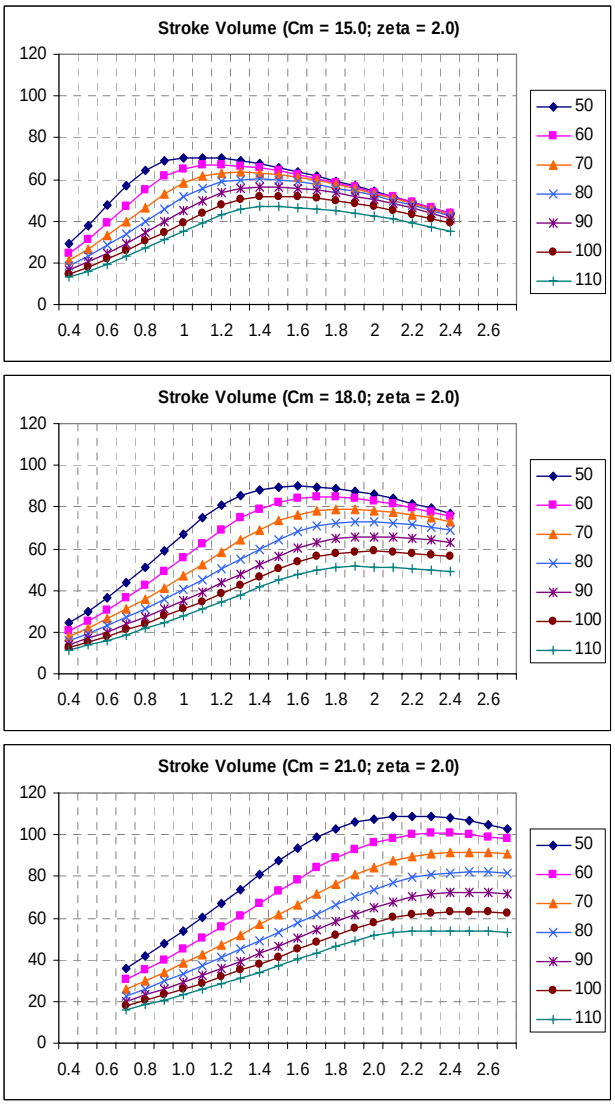

Fig. 11b Variation of the stroke-volume (SV) with wall-thickness (range from 0.4 to 2.7 cm) under various heart rate conditions (50 to 110 BPM) for three different values of mid-wall circumference (15.0, 18.0, and 21.0 cm) and damping ratio equal to 2.0

Another point is worth mentioning here concerning the MAP variations. As the mid-wall circumference is increased from 15.0 to 21.0 cm, the MAP curves become more and more overlapping, indicating that once the left-ventricular reserve has been reached, the left-ventricle becomes incapable of pumping more cardiac output with the increase in HR being offset down by a comparable reduction in stroke volume.

IV. CONCLUSION

In the current approach of left ventricular model, the introduced modifications were aimed at separately modeling the time-excitation and the length- and shape-modulated periodic contraction mechanisms of the ventricular pump. We have combined at the level of the basic muscle unit a second-order viscoelastic time-excitation into nonlinear stress-length muscle characteristics in order to numerically generate the hemodynamic response of the left ventricle. While such complexity has been avoided in lumped and some other modeling approaches, this approach provides an alternative to explore and examine a wider variety of cases, and the individual effects of the various components of the system, mainly at the level of muscle building unit. While other researchers have used global viscoelastic element in their left ventricular modeling approach [14], in this work the viscoelastic element is incorporated at the myocardial electromechanical excitation-contraction process.

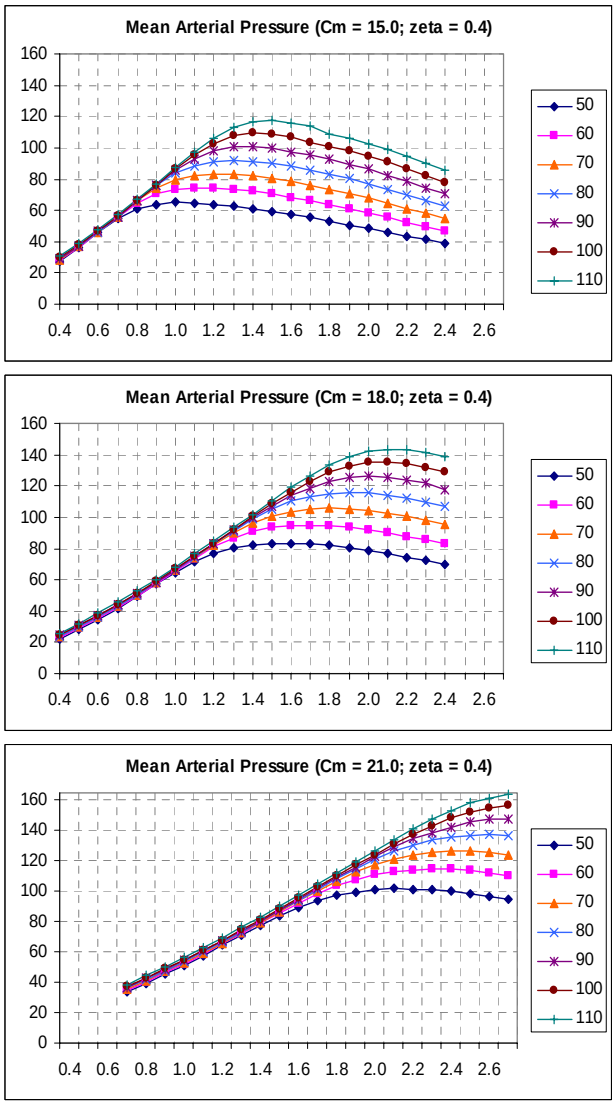

Fig. 12a Variation of the mean-arterial pressure (MAP) with wall-thickness (range from 0.4 to 2.7 cm) under various heart rate conditions (50 to 110 BPM) for three different values of mid-wall circumference (15.0, 18.0, and 21.0 cm) and damping ratio equal to 0.4

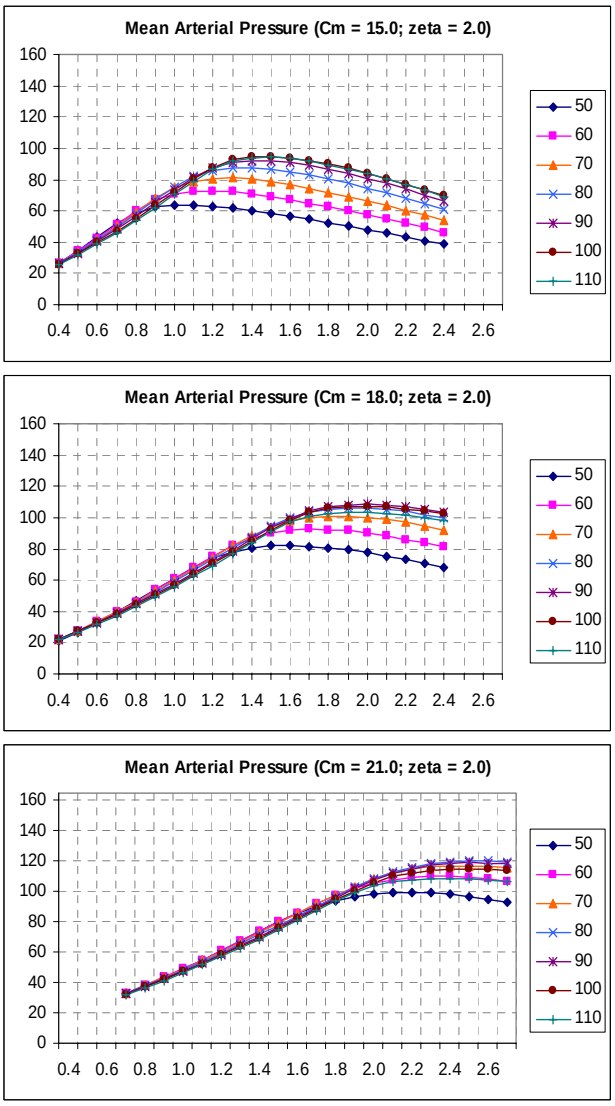

Fig. 12b Variation of the mean-arterial pressure (MAP) with wall-thickness (range from 0.4 to 2.7 cm) under various heart rate conditions (50 to 110 BPM) for three different values of mid-wall circumference (15.0, 18.0, and 21.0 cm) and damping ratio equal to 2.0

The hemodynamic response of the model presented for the case considered agrees with physiological findings. This response depends on the specific values of the stress-length function parameters, as well as on the geometric dimensions of the left ventricle. This is so due to high level of interdependence between the time-variance and nonlinearity of the system. However, the amount of information one can draw from the numerical computation of this model for various cases is worth the time and effort.

The results also show that the nonlinearity of this pulsatile model and the viscoelastic damping ratio of the excitation-contraction coupling mechanism did not alter the well established steady-state relationship among the mean systemic pressure, the cardiac output, and the total peripheral resistance.

Varying ventricular size while venous filling and arterial system parameters are constant cannot be easily performed experimentally. This is an area where mathematical modeling can provide results that are unique. Others have examined mathematically the ventricular function while varying size [15] and [16]. These researchers did not maintain the loading conditions rigorously.

Moreover, these studies do not examine the size effects on the left ventricular performance based on microstructure functions. Similar to some of our results, Gulch and Jacob [16] have shown that stroke volume maximizes with ventricular inner radius. In our previous work [4] and [17], a proposal has been made on the existence of a geometric match, which is the left ventricle is restructured to provide optimal mechanical

match of myofibril dynamics with the external loading conditions. The optimized quantity was proposed to be the myocardial oxygen consumption. The modified model is currently used to reinvestigate this issue, where various types of hypertrophy will be examined.

REFERENCES

[1] H. Suga, "Theoretical analysis of a left-ventricular pumping model based on the systolic time-varying pressure/volume ratio." *IEEE Trans. Biomed. Eng.*, 18(1): 47-55, 1971.
[2] R. Dong, Y. Sun, F. J. Fetter, and S. A. Chiaramida, "Time-varying left-ventricular elastance determined by finite element model." Proceedings of the IEEE 30th Annual Northeast Bioengineering Conference, 188-189, 2004.
[3] G. M. Drzewiecki, E. Karam, and W. Welkowitz, "Physiological Basis for Mechanical Time-Variance in the Heart: Special Consideration of Non-Linear Function." J. Theor. Biol., 465-486, 1989.
[4] E. Karam, "Modeling of Cardiac Growth and Hypertrophy-Regulating Factors." Ph.D. Thesis. Rutgers, The State University of New Jersey, 1992.
[5] E. Karam, A. Abche, and G. M. Drzewiecki, "Left Ventricular Hypertrophy Model Revisited." BIOMEDSIM, University of Balamand, Lebanon, 2003.
[6] G. A. Langer, "Ion fluxes in cardiac excitation and contraction and their relation to myocardial contractility." *Phys. Rev.*, 48: 708-757, 1968.
[7] E. Sonnenblick, D. Spiro, and H. M. Spotnitz, "The ultrastructural basis of Starling's law of the heart. The role of the sarcomere in determining ventricular size and stroke volume." *Am. Heart J.*, 68: 336, 1964.
[8] K. Sunagawa, A. Yamada, Y. Senda, Y. Kikuchi, T. Nakamura, T. Shibahara, and Y. Nose, "Estimation of the hydromotive source pressure from ejecting beats of the left ventricle." *IEEE Trans.Biomed. Eng*., 27: 299-305, 1980.
[9] H.E.D.J. Ter Keurs, W. H. Rijnsburger, van Heuningen, M. J. Najelsmit, "Tension development and sarcomere length in rat cardiac taberculae: Evidence of length-dependent activation." In : *Cardiac Dynamics*. Baan, J., A. C. Arntzenius, and E. L. Yellin (eds.), Martinus Nijhoff Publishers, Boston, 1980.
[10] I. Mirsky, and W. M. Parmley, "Assessment of passive elastic stiffness for isolated heart muscle and intact heart." *Circ. Res.*, 33: 233-243, 1973.
[11] W. M. Parmley, D. L. Brutsaert, and E. H. Sonnenblick, "Effects of altered loading on contractile events in isolated cat papillary muscle." *Circ. Res.*, 24: 521-532, 1969.
[12] J. Ross, Jr., E. H. Sonnenblick, J. W. Covell, G. A. Kaiser, and D. Spiro, "Architecture of the heart in systole and diastole: Technique of rapid fixation and analysis of left ventricular geometry." *Circ. Res.*, 21: 409-421, 1967.
[13] T. Ihara, Y. Yamada, and K. Komamura, "Hemodynamic determinants of left ventricular diastolic function: A model study." 18th Annual Conf. of IEEE EMBS, Amsteram, 1996.
[14] G. Drzewiecki, J-J Wang, J. K-J Li, J. Kedem, and H. Weiss, "Modeling of Mechanical Dysfunction in Regional Stunned Myocardium of the Left Ventricle." *IEEE Trans. Biomed. Eng.*, Vol. 43, No. 12, December 1996.
[15] R. Beyar, and S. Sideman, "Relating Left Ventricular Dimension to Maximum Elastance." *Am. J. Physiol*., 251 (*Regulatory Integrative Comp. Physiol*. 20): R627-R635, 1986.
[16] R. W. Gulch, and R. Jacob, "Geometric and Muscle Physiological Determinants of cardiac Stroke Volume as Evaluated on the basis of Model Calculation." *Basic Res. Cardiol*., 83: 476-485, 1988.
[17] G. M. Drzewiecki, E. Karam, J. K-J Li, and A. Noordergraaf, "Cardiac Adaptation of Sarcomere Dynamics to Arterial Load: A Model of Hypertrophy." *Am. J. Physiol*., 263 (*Heart Circ. Physiol*. 32): H1054-H1063, 1992.